Photoluminescence and Relaxation Processes in MEH−PPV

R. F. Cossiello,[†] E. Kowalski,[‡] P. C. Rodrigues,[§] L. Akcelrud,[§] A. C. Bloise,[⊥] E. R. deAzevedo,[⊥] T. J. Bonagamba,[⊥] and T. D. Z. Atvars*,[†]

Instituto de Química, Universidade Estadual de Campinas, Caixa Postal 6154, 13084-971 Campinas, SP, Brazil; Instituto Tecnológico para o Desenvolvimento LACTEC, Centro Politécnico, 81531-990 Curitiba, PR, Brazil; Departamento de Química, Universidade Federal do Paraná, Centro Politécnico, Caixa Postal 19081, 81531-990 Curitiba, PR, Brazil; and Instituto de Física de São Carlos, Universidade de São Paulo, Caixa Postal 369, 13560-970 São Carlos, SP, Brazil

Received August 11, 2004; Revised Manuscript Received November 22, 2004

ABSTRACT: A detailed description of the thermal relaxation processes in MEH−PPV is reported. Bulk methods such as DMTA were employed in conjunction with other techniques that probe molecular motions, such as fluorescence spectroscopy, thermal stimulated current, and ^{13}C NMR. From the two main transitions observed (glass transition process at 340 K and β-relaxation between 200 and 220 K), it was demonstrated that the first is strongly correlated with the dissociation of a fluorescent emissive interchain complex and that the second relaxation involves movements of the lateral substituents of the polymer backbone and, more specifically, their CH_2 groups. NMR dipolar chemical shift correlation experiments pointed an increasing gain in mobility through the side chain, the lateral carbons close to the aromatic ring being more rigid than those located more distant from the main polymer chain. A kinetic model involving the dissociation of interchains to re-form intrachain excitons was proposed to explain the profiles of the photoluminescence spectra at higher temperatures.

Introduction

Studies of conjugated light-emitting polymers have undegone significant progress since the discovery of the first polymer-based light-emitting diode (PLED).[1] Such studies cover commercial, technological, and scientific interests. One particular type of conjugated polymer, poly(2-methoxy-5-(2-ethylhexyloxy)-*p*-phenylenevinylene) (MEH−PPV), has been the subject of a wide spectrum of studies in recent years, going from the optimization of synthetic pathways to device performance.

An understanding of the photoluminescence (PL) properties in the solid state is a matter of particular interest due to its correlation with the efficiency of electroluminescence devices. Consensual agreements about the MEH−PPV photoluminescence mechanisms have been established: (i) the emission of isolated intrachain excitons is only possible in dilute solutions; (ii) solvents and protocols for film preparation strongly influence the morphology and, consequently, the polymer photophysical properties; and (iii) aggregation depletes the photoemission efficiency.[2] In addition, it has been shown that three types of emission signals can be found in the solid state: (i) intrachain singlet exciton (isolated chromophoric emission) at 16 950−17 540 cm^{-1}, undergoing fast emission on a picosecond time scale;[3−8] (ii) interchain exciton decay (ground-state species involving interactions between segments of different chains), usually taking place at the red edge of the intrachain exciton, ca. 15 630−16 670 cm^{-1}, with lifetimes on the nanosecond scale;[6−10] and (iii) excimer emission (electronic excited-state dimers involving intermolecular interactions between a singlet excited and a nonexcited segment) occurring at 14 280 cm^{-1} (or higher), with a broader band profile.[6,7,9−13] As a consequence of the complexity of photophysical multiple pathways, the photoluminescence decay of MEH−PPV in the solid state under lower excitation density is not a monoexponential process, but involves a faster and a slower component whose relative contributions depend on sample morphology.[9,10,13−17] Furthermore, the photoluminescence quantum yield of the intrachain exciton is higher than those related to the aggregate and excimeric emissions. The contributions of each one of these species to the total emission spectra strongly depend on the film preparation conditions and on the subsequent thermal annealing.[2] Since the properties of conjugated polymers are strongly dependent on morphology, comparisons between reported results should be carefully considered.

In general, the fluorescence intensity of any molecular system is strongly dependent on temperature.[8,18] This is due to the fact that the quantum yield is a ratio between a radiative rate constant and the sum of several other nonradiative rate constants such as vibrational relaxation, internal conversion, intersystem crossing, and energy transfer processes that are, themselves, dependent on temperature.[8,18] For solutions without solvent/polymer specific interactions, the temperature dependences of the nonradiative rate constants are predominantly functions of the intrinsic photophysical properties of the lumophore and of the solvent viscosity.[8,18] On the other hand, the emission efficiency of solid state polymers (intrinsically luminescent or containing fluorescent guests) depends not only on the intrinsic photophysical properties of the lumophore but also on its microenvironment properties, such as polymer chain mobility, interchain interactions, and interchain energy transfer processes.[9,10,13−16] Among these extrinsic properties, polymer relaxation processes are particularly important in changing the relative rates of the radiative and nonradiative processes. Consequently, the temperature dependence of photophysical properties of a

[†] Universidade Estadual de Campinas.
[‡] Instituto Tecnológico para o Desenvolvimento LACTEC.
[§] Universidade Federal do Paraná.
[⊥] Universidade de São Paulo.
* Corresponding author: e-mail tatvars@iqm.unicamp.br; Fax 55-19-37883023; Tel 55-19-37883078.

10.1021/ma048340i CCC: $30.25
Published on Web 01/11/2005

polymeric material cannot be discussed independently of a knowledge of their relaxation processes.

It is widely recognized that the light-emitting performances of optoelectronic devices are strongly affected by thermally induced morphological variations, brought about by field/current Joule effects, in particular. These effects are extremely deleterious to the light emission efficiency and durability of the devices. Thus, it is remarkable that the thermally induced effects in light-emitting polymers, such as MEH−PPV, have not been explored. To our best knowledge, only the thermal induced rheological transitions (the glass transition) of PPV thin films have been studied by shear-modulated scanning force microscopy and correlated with emissive properties.[19] Although the relaxation processes of MEH−PPV have not been reported, the importance of chain mobility has been observed in several studies, without any explanation. For example, some peculiar behavior around 200−220 K was noticed for spectral line narrowing and for the temperature dependence of the absorption and the photoluminescence bands of the polymer.[17] A strong slope change of the electron injection barrier and for the absorption peak was observed below 220 K.[22] The quantum efficiencies of diode-based MEH−PPV increased with a decrease in the temperature, which was later explained as due to the improvement of the charge balance.[20,21] The temperature dependences of both the absorption and the photoluminescence spectra of PPV and MEH−PPV films have shown a red shift of the peak position upon cooling.[23−27] Differences in the magnitude of the shift of absorption and photoluminescence are on the order of kT (thermal energy) and were attributed to conformational changes of the polymer chains. Freezing increases the planarity of the conjugated emitting center and the effective length of the electron delocalization, producing a red shift of the emission spectrum.[28] Thus, although the specific determination of MEH−PPV relaxation processes has not yet been reported, the importance of these processes has been experimentally observed.

The aim of this work is to correlate the MEH−PPV photoluminescence properties at several temperatures with relaxation processes using some complementary and independent techniques: dynamic mechanical thermal analysis (DMTA), thermally stimulated current (TSC), ^{13}C NMR using dipolar chemical shift correlation (DIPSHIFT), and fluorescence spectroscopy. Since several spectral changes occur simultaneously with the polymer relaxation processes, a kinetic model involving the dissociation of interchains to re-form intrachain excitons is proposed, attempting to explain the profiles of the photoluminescence spectra at higher temperatures.

One possible limitation of fluorescence spectroscopy is its lack of ability to assign the secondary relaxation processes to precise segments or groups of the polymer chain. To overcome this problem, we employed one-dimensional 1D-DIPSHIFT NMR. That is a dipolar chemical shift correlation method, where the correlation between the dipolar and chemical shift interactions is used to provide information about molecular reorientations associated with relaxations in solid materials.[27,29,30] Regarding the time scale, DIPSHIFT experiments are most sensitive to motions occurring with rates ranging from 1 to 30 kHz. Molecular motions occurring at these rates scale down the anisotropic $^{13}C-^{1}H$ magnetic dipolar coupling, which usually is of the order of 1−30 kHz, making it possible to distinguish rigid from mobile segments. Because the experiment is performed under magic-angle spinning (MAS), this is achieved for each chemical group along the polymer chain in a high-resolution ^{13}C CP/MAS spectrum. More specifically, the application of the 1D-DIPSHIFT pulse sequence[31] produces an echo at twice the sample rotation period, $2t_r$, whose amplitudes are modulated by $\langle\cos(\omega_{dip}t_1)\rangle$, where $\omega_{dip} = \delta_{dip}(3\cos^2\theta - 1)/2$, δ_{CH} is the anisotropy parameter for the heteronuclear dipolar interaction, θ is the angle between the CH bond and the static magnetic field $\vec{B}_0$, and the evolution period t_1[30] is the time in which the carbon magnetization evolves under the CH dipolar coupling, $\omega_{dip} = 2\pi\upsilon_{dip}$. Therefore, by measuring the signal amplitude as a function of t_1, typical curves whose shape depends on υ_{dip} are obtained, allowing estimating this parameter. If molecular motions occurring with rates higher than 1 kHz are present, the strength of the anisotropic dipolar coupling is partially or totally averaged, and as a result, motional averaged anisotropic dipolar CH coupling $\langle\omega_{dip}\rangle = 2\pi\langle\upsilon_{dip}\rangle$ is measured in DIPSHIFT experiments.

Experimental Section

Materials. MEH−PPV was purchased from Aldrich, with a molecular weight of 86 kg mol^{-1}, according to the supplier. It was used as received. Toluene was supplied from Merck 99.5% of purity and chloroform was from Vetec, Brazil (99.8%). The solvents were dried using molecular sieves (4 Å). Fresh solutions were used for each film preparation.

Films were spin-coated at 3000 rpm during 30 s in a Headway Research Inc. model PWM32 spinner. A thickness of 800 nm was determined by inspecting the film fracture surfaces with a JEOL JSM-6360LV scanning electron microscope. The surface was sputtered with gold/palladium (80/20) alloy in a Bal-Tec MED 020 MCS 010 casting system. Images were recorded with an accelerating voltage of 10 kV.

Methods. Steady-state fluorescence spectroscopy was performed using a system described elsewhere.[33] Samples were excited by a high-pressure mercury lamp arc (200 W) whose excitation wavelength of 21 280 cm^{-1} was selected by a Jarrell-Ash 0.25 mm monochromator. Low-density excitation was employed to reduce the probability of any kind of nonlinear optical effects. Films (1 × 1 cm) were inserted between two quartz windows held in an optical support. The optical holder within the cryo-system (APD Cryogenics) was positioned to minimize the scattering of light from the excitation beam in a way to stay immobile.

The samples were maintained under a dynamic vacuum of 10^{-4} Torr during the measurements. Temperature was changed from 40 to 400 K in steps of 10 K by a digital temperature controller (Scientific Instruments model 9650) and allowed to attain equilibrium for 5 min between each measurement. One spectrum was recorded at each temperature, and because all of the experimental conditions were maintained constant, the emission intensities were comparable over the entire experiment.

A dynamic mechanical thermal analysis DMA 242-Netzsch Thermisch Analyse equipment was used to perform the thermal analyses. The dynamic mechanical characterization (DMA) was performed in the tension mode, under a steady load of 1.78 MPa and a dynamic stress of 1.98 MPa, under a nitrogen flow of 50 mL/min. The scans were made over the temperature interval of 170−420 K at a heating rate of 2 K/min at frequencies of 1, 5, 10, 16, 20, 25, and 33 Hz. Each sample was cut from chloroform cast films to a small rectangular sample, 10 mm long, 4.5−5.2 mm wide, and about 0.02 mm thick.

The activation energy was calculated by plotting the frequency f vs T^{-1} for the loss modulus (E'') according to the Arrhenius law (eq 1):

$$f = f_0 \exp(-E/RT) \quad (1)$$

where f is the frequency (Hz), f_0 is the preexponential factor (Hz), E is the activation energy (J mol^{-1}), T is the absolute temperature (K), and R is 8.32 J K^{-1} mol^{-1}.

Nuclear magnetic resonance (NMR) experiments were performed using a Varian Inova spectrometer at ^{13}C and ^{1}H frequencies of 100.5 and 400.0 MHz, respectively. A Varian 7 mm MAS double-resonance probe head with variable temperature (VT) was used. The spinning speed was controlled by a Varian pneumatic system that ensures a rotation stability of ±2 Hz. Typical $\pi/2$ pulses lengths of 3.5 and 4.0 μs were applied for ^{13}C and ^{1}H, respectively. A proton decoupling field strength of 60 kHz, cross-polarization time of 1 ms, and recycle delays varying between 3 and 5 s were used. The temperature dependence of ^{13}C−^{1}H dipolar couplings were measured using 1D dipolar chemical shift correlation (1D-DIPSHIFT) experiments.[34,35] ^{1}H−^{1}H homonuclear decoupling was achieved by the frequency−switch−Lee−Goldburg (FSLG) pulse sequence performed with phase modulation and a field strength of approximately 80 kHz.[34,35] The maximum evolution time in the 1D-DIPSHIFT experiments was 191.5 μs, which corresponds to a spinning frequency of 5222 Hz. The scaling factor of the FSLG sequence was experimentally obtained using alanine and glycine as reference samples, whose dipolar coupling values for CH, CH_2, and CH_3 groups are 13.7, 16.3, and 22.8 kHz, respectively.

Thermally stimulated current (TSC) experiments were performed with samples in the form of square thin films (25 × 25 mm), 50 mm thick, covered on both sides with aluminum electrodes of about 20 cm in diameter, deposited by evaporation. An Edwards cryogenic chamber and high-vacuum system was used in conjunction with a Gefran temperature controller, model 3300. The electric current on depolarization was measured by a Keithley model 617 electrometer. Temperature and current data were collected by a computer. The following steps were performed in the measurements: (i) the temperature was raised to 393 K, and a polarization electric field of 20 MV/m was applied during 30 min; (ii) under the action of the electric field the sample was cooled to 77 K at 5 K/min; (iii) a short circuit until a current of 10^{-15} A was registered; and (iv) the temperature increase up to 450 K at rate of 5 K/min and the depolarization electric current values were registered as a function of temperature. The vacuum in the system was held at 10^{-7} Torr throughout the experiment. The activation energy was calculated using the method of Lei et al.[38] The thermally stimulated current is expressed by

$$I = C' \exp\left[-\left(\frac{A}{kT}\right) - D\int_{T_0}^{T}\exp\left(-\frac{A}{kT'}\right)\mathrm{d}T'\right] \qquad (2)$$

where $C' = P_0S/\tau_0$ and $D = 1/h\tau_0$; T is the absolute temperature, k the Boltzmann constant, and A the activation energy corresponding to a determined relaxation process. C' and D are coefficients independent of T and A. With some mathematical manipulation one gets

$$C = a_1 + \sum_{n=0}(1 - {a_2}^{n+2}\mathrm{e}^{-C})\frac{(n+1)!}{C^n}\,{a_3}^n(-1)^n \qquad (3)$$

where $a_2 = T_i/T_p$, $a_3 \equiv (T_p - T_i)/T_i$; T_p is the temperature corresponding to the relaxation and T_i the lower temperature immediately closer to T_p; t_0 is the relaxation time, h is the heating rate, S is the electrode area, and P_0 is the initial sample polarization.

Using eq 3, C can be numerically determined and the activation energy is estimated according to

$$A = C\frac{kT_pT_i}{T_p - T_i} \quad \text{and} \quad \tau_0 = \frac{kT_p{}^2\mathrm{e}^{-A/kT_p}}{hA} \qquad (4)$$

Results and Discussion

Photoluminescence Spectra. Figure 1 depicts the photoluminescence (PL) spectra at several temperatures, from 40 to 410 K, of spin-coated films of MEH−PPV from both toluene and chloroform solutions. Fluorescence spectra at higher temperatures (T > 310 K) are broader, centered at 16 950 cm^{-1}, with a longer red-edge tail. The blue-shifted peak can be assigned to intrachain excitons and the red-edge emission to interchain species.[5−10,13−17] Spectra at lower temperatures (T < 220 K), centered around 16 390 cm^{-1}, were assigned to interchain excitons of MEH−PPV, as previously observed for concentrated solutions.[5−8] No emission around 14 285 cm^{-1} was found, indicating complete absence of emitting excimers.[39] In addition to the temperature dependence of the spectral profile, there is also an increase in the emission intensity at the blue edge, which is in agreement with the expected higher quantum yield of the intrachain excitons as compared to the interchain species.[8−10,13−17]

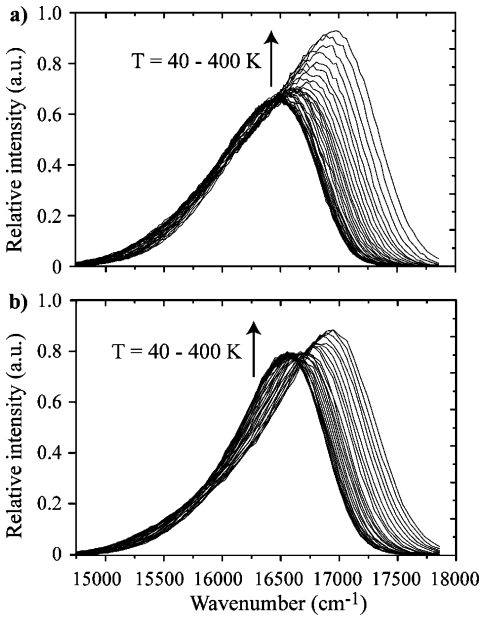

Figure 1. Photoluminescence spectra at several temperatures (from 40 to 400 K) for MEH−PPV spin-coated films: (a) spun from chloroform; (b) spun from toluene. λ_{exc} = 21 270 cm^{-1}.

It has been observed that the spectral profile of MEH−PPV varies with temperature and with the solvent used to spin the polymer solution, demonstrating a memory effect from the conformation in solution even after annealing the samples. The narrower spectra found for films spun from toluene are compatible with a more ordered material, while a broader distribution of conformations is found for films spun from chloroform.[8−10,13−17] The full width at half-maximum (fwhm) (Figure 2a) is a parameter that can describe both the heterogeneity of the microenvironment around the fluorophore and the spectral overlap resulting from the presence of different intrachain conformations.[40] Both effects are effectively present in MEH−PPV films, broadening the emission band. Additionally, the photoluminescence spectrum is further broadened by the presence of interchain species. Consequently, the fwhm values in the range of 1000−900 cm^{-1} are orders of magnitude larger than expected for homogeneous broadening of species with decays on the pico- to nanosecond time scale. Therefore, the resulting spectral shape reflects the cooperative effects of homogeneous and inhomogeneous broadening, conformational disorder, and multiple species decays.

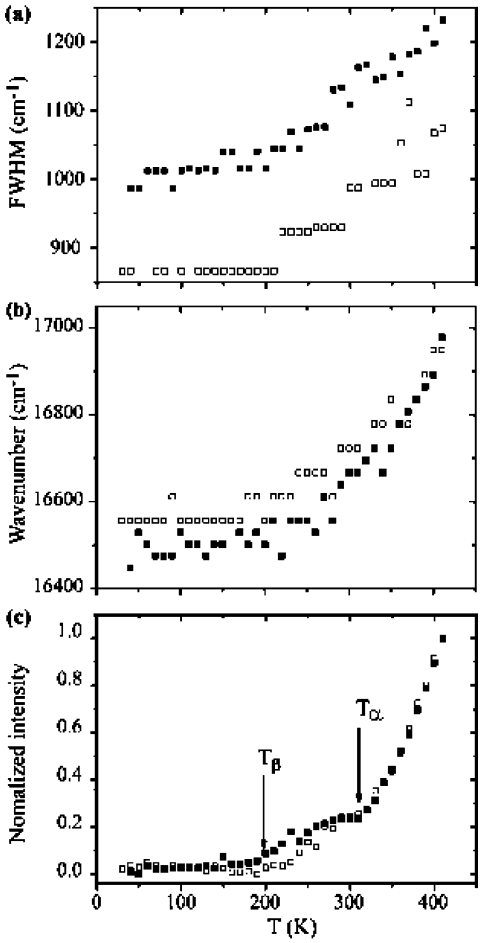

Figure 2. (a) Fwhm, (b) photoluminescence peak maxima (cm^{-1}), and (c) integrated and normalized intensity, $I_F(T)/I_F(T_0)$, at several temperatures for MEH−PPV films: spun from toluene (□) or spun from chloroform (■). λ_{exc} = 21 270 cm^{-1}.

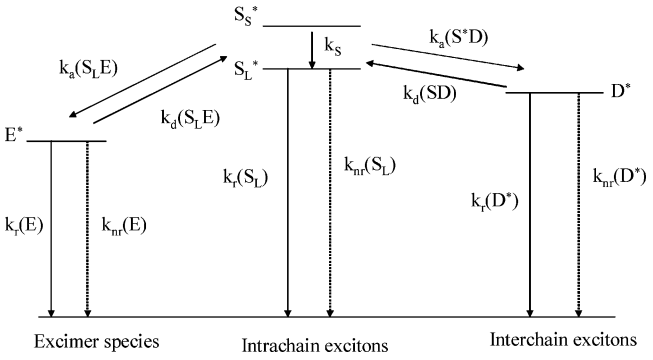

Figure 3. Kinetic scheme for the fluorescence decays of MEH−PPV films, where M is the ground-state chromophore, M* is an excited-state species, I is the intrachain exciton, D* is the excited-state aggregate, k_{nr} and k_r are the radiationless and radiative rate constants, respectively, $k_a(S^*_LD)$ is the rate constant for the intrachain exciton forming an excited dimer, and $k_d(S^*_LD)$ is the rate constant for the aggregated dissociation re-forming the intrachain exciton.

There are some hypotheses postulated to explain the blue shift of the photoluminescence spectra at higher temperatures (Figures 1 and 2b). Assuming that only intrachain excitons are responsible for the photoluminescence, the blue shift can be attributed to (i) thermally induced torsional motions shortening the conjugation lengths and (ii) differences in the Huang−Rhys coupling factors (S) for chains with distinct conjugation lengths, leading to differences in the relative intensities of the zero- and higher-order phonons, producing changes in the spectral profile.[17,26] Although these possibilities explain the blue shifts at higher temperatures, these properties cannot explain the blue shift and intensity enhancements for increasing temperatures. To explain the simultaneous change of the peak position and emission intensity, we have assumed that different species are emitting in each temperature range, in agreement with data reported for PPV.[17,26] The emission of isolated PPV chains at lower temperatures (10 K) is red-shifted by at least 400 cm^{-1} as compared to that at higher temperatures (300 K).[30] This effect cannot be explained by simple thermal population of states, which is only 208 cm^{-1}. The difference between the emission maxima at 300 and 40 K is 220 cm^{-1}, which, in principle, could be attributed to the thermal population of states. However, the peak position is not a continuous function of the temperature increment: from 40 to 200−220 K the peak position is essentially constant, with a continuous spectral shift being observed from 300 to 400 K (Figure 2b).

The dependence of the integrated and normalized photoluminescence intensities on temperature is shown in Figure 2c. Each intensity value was taken as the ratio between the integrated fluorescence (area under the entire spectrum plotted in wavenumbers) at a given temperature and the integrated intensity at the lowest measured temperature, $I_F(T)/I_F(T_0)$. We have considered $I_F(T_0)$ as the value measured at 40 K, although rigorously $I_F(T_0)$ should be at 0 K. Taking into account that the emission intensity is almost temperature independent below 140 K, we can assume that those radiationless processes strongly dependent on temperature are inhibited below this temperature.[8,18]

Two isoemissive points were found for both samples, around 16 714 and 16 605 cm^{-1}, suggesting that some kind of thermal equilibrium involving two different species might be operating. Assuming different species emitting with distinct efficiencies from 30 up to 410 K, we could explain the simultaneous blue shift and higher intensity upon heating, considering the kinetic scheme depicted in Figure 3, where the dissociation of some interchain species gives rise to an intrachain exciton. According to this scheme, and in absence of excimeric species, some short chains can be vibronically excited (S_S*) and rapidly relax to longer intrachain electronically excited states (S_L*) through vibrational relaxation and internal conversion (k_S). This S_L* species can decay nonradiatively to an interchain trap producing an interchain exciton (D*) ($k_a(S_L{}^*D)$) or can decay to an interchain excimer (E*) ($k_a(S_L{}^*E)$). This last pathway was ruled out because excimer emission at 700 nm was not observed. On the other hand, this longer intrachain species (S_L*) can decay radiatively ($k_r(S_L)$) or nonradiatively ($k_{nr}(S_L)$). When the excited intrachain segments undergo faster radiative decay to the electronic ground state, the observed emission is at $h\nu_{F(L)}$ = 16 950 cm^{-1} (Figure 1). This is the most important emission at temperatures above 320 K. The excited interchain species (D*) could also decay radiatively (k_r(D*) or nonradiatively (k_{nr}(D*) (Figure 3). When the decay is radiative (D* → D), the emission takes place at the red edge of the intrachain excitons ($h\nu_{F(D)}$ = 16 390−16 500 cm^{-1}) (Figure 1). This is the higher intensity emission occurring below 200 K and is responsible by the longer red edge tail of the emission spectrum above this

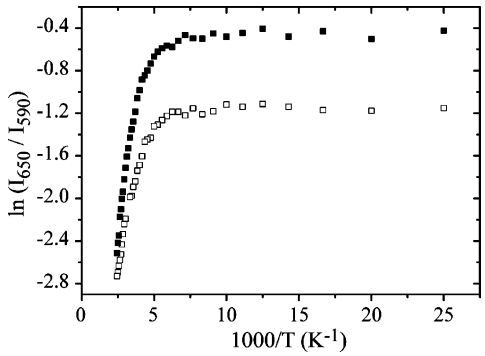

Figure 4. Arrhenius plot for the interchain/intrachain intensity ratio (I_{15385}/I_{16950}) vs $1/T$ for MEH−PPV films spun from chloroform (■) and toluene (□). $\lambda_{em}(D) = 15\ 385\ cm^{-1}$ and $\lambda_{em}(S_L) = 16\ 950\ cm^{-1}$.

temperature. Because of the higher relative quantum yield of the intrachain relative to the interchain excitons, the integrated intensity at higher temperatures increases, even though the radiationless rates (such as internal conversion, vibrational relaxation, and intersystem crossing, $k_{nr}(S,L,D)$) also become more efficient.[8,18]

Therefore, we considered that the relative intensity changes at 16 950 and 16 390 cm^{-1} depend on the population of intrachain and interchain species, and for $T > 300$ K the dissociation of interchain species becomes an efficient process. The temperature dependence for interchain dissociation can be described by the ratio of the emission intensity at 16 950 cm^{-1} (where the intrachain is preferentially emitting) and at 16 390 cm^{-1} (where we are assuming that only the interchain exciton is contributing to the emission signal). We assume a simplified kinetic model where chain segments form interchain species (D*) with a rate constant $k_a(S^*_LD)$ and undergo dissociation, re-forming intrachain excitons, S_L^*, with a rate constant $k_d(S^*D)$.[8,18,26,41] This kinetic scheme is similar to that developed for the temperature dependence of excimer emission.[26] According to our experimental data, at higher temperatures ($T > 320$ K) the efficiency of the interchain D* emission is lower than of the intrachain excitons, $k_d \gg k_D$ (rate constants for the interchain deactivation include radiative and radiationless rates). At lower temperatures ($T < 200$ K), $k_a(S^*_LD) \gg k_d(S^*D)$ and $k_a(S^*_LD) \gg k_{S(L)}$ where $k_{S(L)} = k_r(S_L) + k_{nr}(S_L)$ is the rate constant for the intrachain deactivation including radiative and radiationless rates, and the emission arises preferentially from the interchain excitons. Considering this as a typical example of chemical equilibrium involving association and dissociation, the temperature dependence of the intensity ratio $I_{F(D^*)}/I_{F(SL^*)}$ can be represented as an Arrhenius plot (Figure 4), where the emission for D* and S_L takes place at 15 380 and 16 950 cm^{-1}, respectively.

All plots in Figure 2 displayed two distinct temperature ranges for the changes in spectral behavior: at 210 ± 10 K producing changes with smaller magnitudes and at 330 ± 10 K producing changes with greater magnitudes, where interchain dissociation is taking place. Usually, slope changes of fluorescence intensity can be attributed to changes in nonradiative rate constants and in polymer systems to polymer relaxation processes.[9,10,13−15] Smaller changes may be assigned to motions of smaller groups or lateral segments noneffiCiently coupled with the polymer backbone or with the conjugated chain. Larger changes are attributed to motions of longer segments. Thus, we assign the lower temperature process, occurring at 210 ± 10 K, to a secondary process (β-relaxation) and the higher temperature process, at 330 ± 10 K, to the glass transition (α-relaxation). The net result that can be obtained from the above discussion is that the glass transition and the dissociation of aggregated emitting species are strongly correlated events.

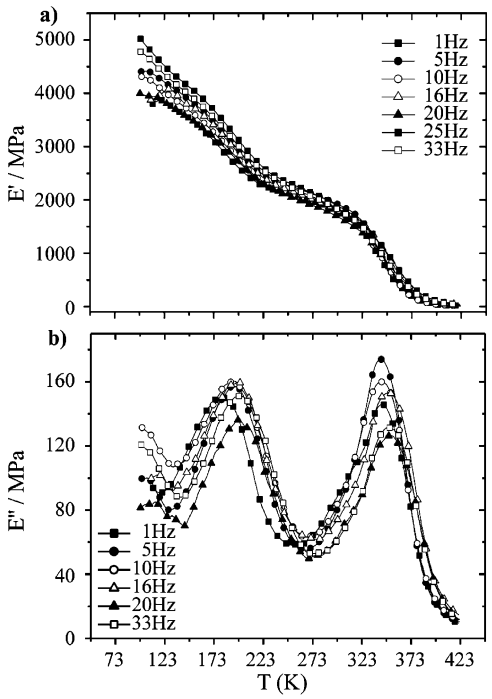

Figure 5. DMTA plots for a film of MEH−PPV at several frequencies.

Dynamical Mechanical Thermal Analysis. To gain further insight into the role played by chain mobility on the photophysical changes occurring at 330 ± 10 and 210 ± 10 K, DMTA experiments were run from 140 to 420 K (Figure 5). Both storage and loss moduli showed two broad relaxation processes: at 340 and at 220 K, which we previously assigned to the α- and β-relaxation processes, respectively. The relaxation temperatures were in the same range as those determined by fluorescence spectroscopy. The α-relaxation process observed by DMTA was also consistent with that previously determined by DSC, $T_g = 338$ K. Arrhenius plots (Figure 6) with data from experiments run at several frequencies gave the activation energy for each relaxation process as 85.4 and 29.1 kJ mol^{-1} K^{-1}, respectively, for T_g and β-relaxation processes, indicating that the β-relaxation involves shorter segments of the polymer chain.

Thermal Stimulated Current. In addition to the DMTA we have also measured the relaxation processes by depolarization of thermal stimulated current using samples which were polarized at 390 and 430 K. The depolarization currents were recorded (Figure 7), showing two main relaxation processes: one at a lower temperature range, from 100 up to 240 K, and another at a higher temperature range, from 300 to 370 K. Both sets of transitions were located at the same temperature ranges as those observed by DMTA and photoluminescence, which were previously assigned to β-relaxation and glass transition. Each one of these transitions exhibited subcomponents associated with sequential

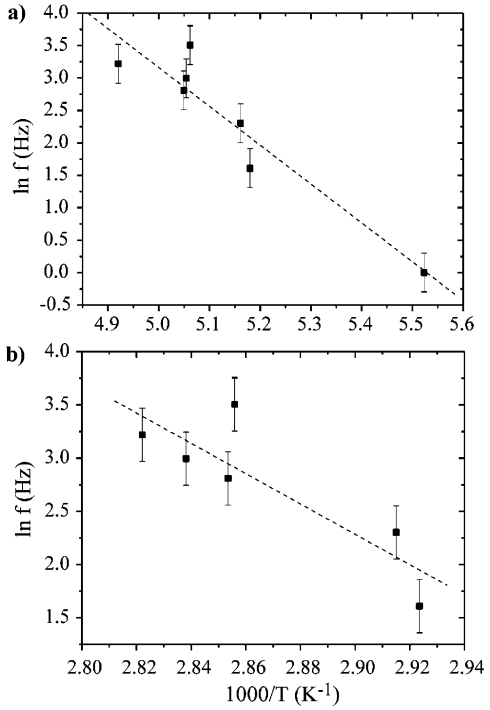

Figure 6. Arrhenius plots for the β (a) and α (b) relaxations by DMTA.

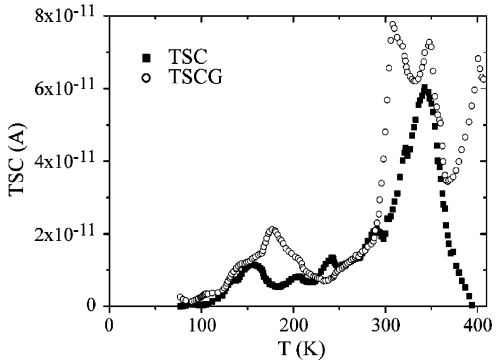

Figure 7. TCS plots for a MEH−PPV spin-coated film polarized at 390 (■) and 430 K (○).

movements of polar segments of the polymer, distinctly polarized by the electrical filed. The assignment of each subtransition requires further detailed experiments. The calculated activation energies for the glass transition and β-relaxation processes were 62.4 and 22.5 kJ mol^{-1} K^{-1}, respectively. The activation energy values of the β-relaxation obtained by TSC and DMTA (29.1 kJ mol^{-1} K^{-1}) are in very good agreement, whereas those obtained for the glass transition differ of about 20 kJ mol^{-1} K^{-1} (85.4 kJ mol^{-1} K^{-1} for DMTA). This difference related to long-range motions is probably associated with the mechanisms involved with the relaxation processes; i.e., DMTA involves the entire bulk while TSC involves movements of the polar groups of the polymer chain.

Although TSC, DMTA, and fluorescence spectroscopy identified two relaxation processes in the same temperature ranged, only PL was able to demonstrate that the higher temperature process involved interchain movements producing dissociation of the interchain complex. On the other hand, no microscopic details can be inferred for the β-relaxation, apart from the indication that it is correlated with the side groups, due to the

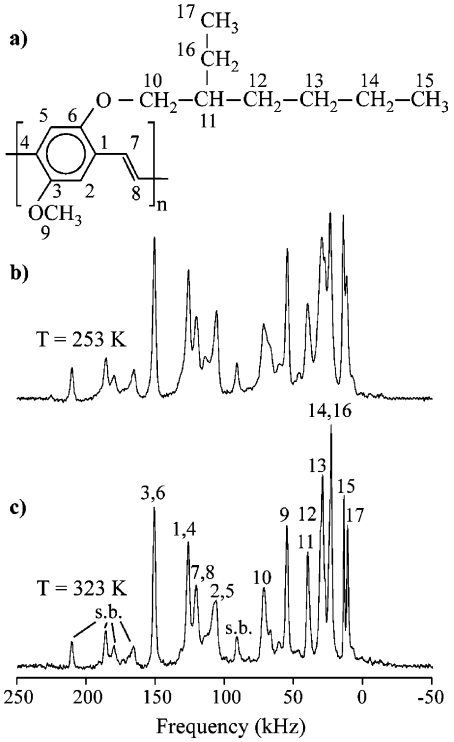

Figure 8. MEH−PPV repetitive unit (a) and magic-angle-spinning NMR spectra of MEH−PPV with the corresponding line assignments at (b) 253 and (c) 323 K.

smaller magnitude of the spectral, TSC, and DMTA signals.

^{13}C NMR Analysis. The identification of the isotropic chemical shift for each chemical group in the ^{13}C CP/MAS spectrum of MEH−PPV was achieved on the basis of typical chemical shift values. The repetitive units and typical ^{13}C CP/MAS spectra of MEH−PPV at 253 and 323 K are shown in Figure 8. Cross-polarization experiments with dipolar dephasing were also applied to distinguish protonated from nonprotonated carbons.[35] This helped in the identification of the main chain carbon resonances, which appear with considerable superposition in the NMR spectra. Thus, the line at 126 ppm was attributed to phenylene carbons 1 and 4, while the line at 120 ppm was attributed to the CH vinylene groups (carbons 7 and 8). The lines at 11 and 23 ppm were attributed to carbon 16 and 17 belonging to the ethyl side group, while the peaks at 14, 23, ∼29, 39, and 72 ppm were ascribed respectively to carbons 15, (16 and 14), (13 and 12), 11, and 10, belonging to the hexyloxy side group. The resonance at 55 ppm is typical of methoxy groups, carbon 9. Finally, the lines at ∼106 and 151 ppm were identified as belonging to the CH (carbons 2 and 5) and CO (carbons 3 and 6) phenylene carbons, respectively.

At 323 K the lines corresponding to the side-group carbons are narrower than at 253 K, showing an increase in side group mobility at the higher temperature. Comparing the line corresponding to the side-group carbons at both temperatures, it was possible to observe different line widths, which relate to differences in rates of motion along the side chain. Specifically, on the basis of the line width for the peak attributed to carbons 12 and 13 compared with carbons 14 and 16 in the spectrum at 253 K, it is possible to conclude that the mobility of the latter is faster than the former. Besides, the lines are broader for carbons nearer the

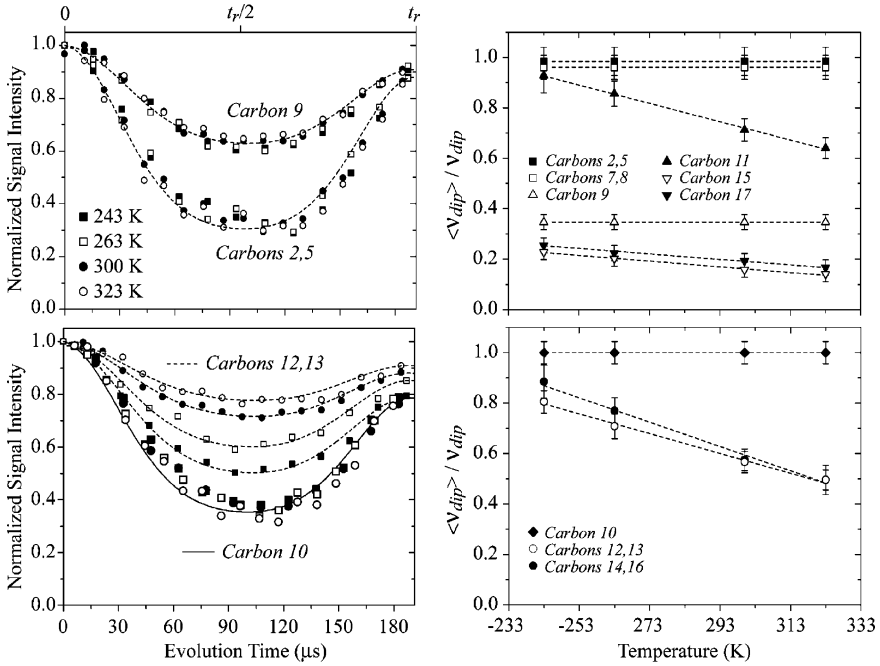

Figure 9. (a) Experimental and simulated DIPSHIFT curves for carbons 2, 5, and 9 vs temperature in MEH−PPV. The curves are presented for a full rotor period with T_2 effects included in the simulation. (b) Same as in (a) for carbons 10, 12, and 13. (c, d) Normalized averaged dipolar couplings vs temperature for protonated carbons.

main chain, narrowing systematically for the carbons closer to the end of the side group, indicating a slight mobility gradient along the side chains.

Molecular Motions in MEH−PPV Probed by DIPSHIFT Experiments. As mentioned, a study of MEH−PPV dynamics was carried out using 1D-DIPSHIFT experiments. Simulation of the DIPSHIFT curves and corresponding fit of the experimental data provided an estimation of the averaged dipolar coupling frequency, $\langle \nu_{dip} \rangle$. T_2 effects, also considered in the simulations, were responsible for the partial decay of the 1D-DIPSHIFT intensities at t_r.

Figure 9 shows the temperature dependence of the averaged dipolar coupling frequency, normalized by the rigid limit value, $\langle \nu_{dip} \rangle / \nu_{dip}$, for several carbons along the side chain.

The $\langle \nu_{dip} \rangle / \nu_{dip}$ curves vs temperature obtained for carbons 2, 5, and 9, as well as the rate $\langle \nu_{dip} \rangle / \nu_{dip} \sim 1$ in MEH−PPV, demonstrate the absence of molecular motions in the polymer backbone on a kilohertz time scale. Similar behavior was observed for the other protonated carbons in the main chain (not shown).

Particular attention should be taken with the methoxy carbon, which presents $\langle \nu_{dip} \rangle / \nu_{dip} \sim 0.33$, even though CH_3 groups have the highest rigid lattice dipolar coupling. This is typical for segments executing anisotropic motions, which partially average the corresponding dipolar coupling. Actually, these experimental curves are reproduced using a dipolar coupling of 7.6 kHz, which is 3 times smaller than that expected for rigid CH_3 groups (22.8 kHz), suggesting the presence of CH_3 rotations around the C_3 axis occurring at frequencies higher than 30 kHz.

Complementarily, a clear temperature dependence of $\langle \nu_{dip} \rangle / \nu_{dip}$ was observed in the curves of side-group carbons, as for example, carbons 14 and 16. This demonstrated the presence of thermally activated molecular motions in the MEH−PPV side chain. For CH_3 side-group carbons, $\langle \nu_{dip} \rangle / \nu_{dip}$ decays as a function of temperature, and its value was always smaller than 0.33, suggesting that the CH_3 side-group carbons experiment extra dynamics associated with the bulk motion of the side chain. This was confirmed by the behavior of the side-group CH carbons, where $\langle \nu_{dip} \rangle / \nu_{dip}$ decreases monotonically with temperature, showing the increasing gain of mobility of this group as a function of temperature.

Another interesting item to be pointed out is the temperature dependence of the DIPSHFT curves for CH_2 groups at different positions in the side chain. Because all the signals analyzed in this case are from CH_2 groups, due to the temperature independence of the curve for carbon 10, it is advantageous to perform the normalization using the averaged CH coupling of this group, ν_{dip}^{C10}. By doing so, the dynamic behavior along the side chain was studied in comparison with the dynamics of carbon 10. The temperature dependence of the parameter $\langle \nu_{dip} \rangle / \nu_{dip}^{C10}$ for all side chain CH_2 groups is shown in Figure 9. The $\langle \nu_{dip} \rangle / \nu_{dip}^{C10}$ temperature dependences also have the same trend; i.e., while it is constant for carbon 10 it decreases monotonically with temperature for the other CH_2 groups. Thus, these results also point to an increasing mobility through the side chain with temperature.

At this point it is worthwhile to compare the frequency scales to which experiments are sensitive. As mentioned before, NMR experiments, such 1D-DIPSHIFT, are sensitive to motions occurring with rates ranging from 1 to 30 kHz, which are higher than the usual frequencies where DMTA experiments are performed (hertz to few kilohertz). Then, because the rate of the molecular motions is associated with temperature and frequency, the same molecular relaxation in each experiment will not necessarily appear at the same temperature. Similar time-correlated effects can be observed when comparing fluorescence spectroscopy and TSC (both involving reorientation of dipole moments) and NMR data. The major differences rely on the fact that DIPSHIFT NMR experiments measures CH bond

reorientation, TSC measures the rate constants for reorientation of the dipole moment after a prepolarization, and fluorescence spectroscopy measures the temperature dependence of a ratio among radiative and nonradiative decays taking place on a nano- to picosecond time scale.

Thus, we cannot expect that the activation energy for all of these processes should be similar, although, in general, we observed a narrow temperature range where decay rates undergo some changes. When comparing NMR with the time scale of PL measurements, the frequency range was always quite different if we consider a correlation with the radiative rate constants. The PL time scale is from pico- to nanoseconds, faster than magnetic resonance. When compared with nonradiative pathways, the time scale is even faster (from pico- to sub-picoseconds). Nevertheless, what we observe in PL are relative changes of the rate constants, which are produced by chain motions and which should take place on the same time scale as the NMR signals because they involve the same type of movements, rotation of groups of the polymer chain. Thus, even though the detected relaxation temperatures in each technique are in the same range, the activation energies for the processes could be different due to the phenomenological differences involved.

Conclusions

This work identified two relaxation processes in solid-state MEH−PPV. DSC, DMTA, TSC, and fluorescence spectroscopy showed that the glass transition takes place in the 330−340 K range. This is the temperature range where MEH−PPV is usually annealed and where there are remarkable changes of the morphology, such as the surface roughness. In addition to the already demonstrated morphological changes, we demonstrated by fluorescence spectroscopy that the glass transition process involves dissociation of interchain species. We also observed by DMTA, TSC, fluorescence spectroscopy, and NMR that MEH−PPV undergoes a secondary relaxation process around 220 K that we called β-relaxation. This is the temperature where some unexplained behavior of several of the MEH−PPV electrical and optical properties can be noted. Although TSC and fluorescence spectroscopy suggest that this is a very complex process involving the lateral substituents of the backbone, only NMR unequivocally showed that the substituents are really involved. More specifically, CH_2 carbons 12−17 are the most important segments relaxing in this temperature range, while groups directly attached to the phenylene ring do not to contribute the β-relaxation process.

Acknowledgment. T.D.Z.A., R.F.C., A.C.B., E.R.d.A., and T.J.B. thank FAPESP, CNPq, and MCT/PADCT/IMMP for fellowships and financial support. L.A., P.C.R., and A.C.B. thank CNPq and MCT/PADCT/IMMP for fellowships and financial support. We also acknowledge Prof. Carol Collins for useful discussions.

References and Notes

(1) Akcelrud, L. *Prog. Polym. Sci.* **2003**, *28*, 875.
(2) Nguyen, T.-Q.; Martini, I. B.; Liu, J.; Schwartz, B. J. *J. Phys. Chem. B* **2000**, *104*, 237.
(3) Samuel, D. W.; Rumbles, G.; Collison, C. J.; Friend, R. H.; Moretti, S. C.; Holmes, A. B. *Synth. Met.* **1997**, *84*, 497.
(4) Whitelegg, S. A.; Buckley, A.; Rahn, M. D.; Fox, A. M.; Bradley, D. D. C.; Palsson, L. O.; Samuel, I. D. W.; Webster, G. R.; Burn, P. L. *Synth. Met.* **2001**, *119*, 575.
(5) Sartori, S. S.; Feyter, S.; Hofkensn, J.; Auweraer, M. V.; Schryver, F.; Brunner, K.; Hofstraat, J. W. *Macromolecules* **2002**, *36*, 500.
(6) Dogariu, A.; Vacar, D.; Heeger, A. J. *Phys. Rev. B* **1998**, *58*, 10518.
(7) Collison, C. J.; Wan, W. C.; Rothberg, L.; Hsich, B. R. *J. Phys. Chem. A* **1999**, *103*, 2394.
(8) Birks, B. *Photophysics of Aromatic Molecules*; Wiley: New York, 1970.
(9) Klopffer, M.-H.; Bokobza, L.; Monnerie, L. *Macromol. Symp.* **1997**, *119*, 119.
(10) Luo, C.; Atvars, T. D. Z.; Meakin, P.; Hill, A. J.; Weiss, R. G. *J. Am. Chem. Soc.* **2003**, *125*, 11879.
(11) Jakubiak, R.; Collison, C. J.; Wan, W. C.; Rothberg, L.; Hsich, B. R. *J. Phys. Chem. A* **1999**, *103*, 2394.
(12) Lim, S.-H.; Bjorklund, T. G.; Gaab, K. M.; Bardeen, C. J. *J. Chem. Phys.* **2002**, *117*, 454.
(13) Jenekhe, S. A.; Osaheni, J. A. *Science* **1994**, *265*, 765.
(14) De Deus, J. F.; Andrade, M. L.; Atvars, T. D. Z.; Akcelrud, L. *Chem. Phys.* **2003**, *297*, 177.
(15) Schurr, O.; Yamaki, S. B.; Wang, C.; Atvars, T. D. Z.; Weiss, R. G. *Macromolecules* **2003**, *36*, 3485.
(16) Vigil, M. R.; Bravo, J.; Baselga, J.; Atvars, T. D. Z. *Curr. Org. Chem.* **2003**, *7*, 197.
(17) Sheridan, A. K.; Lupton, J. M.; Samuel, I. D. W.; Bradley, D. D. *Chem. Phys. Lett.* **2000**, *322*, 51.
(18) Lakowicz, J. R. *Principles of Fluorescence Spectroscopy*; Academic Press: New York, 1999; Chapter 4.
(19) Gray, T.; Buenviaje, C.; Overney, R. M.; Jenekhe, S. A.; Zhen, L.; Jen, A. K. Y. *Appl. Phys. Lett.* **2003**, *83*, 2563.
(20) Bozano, L.; Tutle, S. E.; Carter, S. A.; Brock, P. J. *Appl. Phys. Lett.* **1998**, *73*, 3911.
(21) Bozano, L.; Carter, S. A.; Scott, J. C.; Malliaras, G. C.; Brock, P. J. *Appl. Phys. Lett.* **1999**, *74*, 1132.
(22) Lupton, J. M.; Samuel, I. D. W. *Synth. Met.* **2000**, *111*, 381.
(23) Yu, J.; Hagashi, M.; Lin, S. H.; Liang, K. K.; Hsu, J. H.; Fann, W. S.; Chao, C.-I.; Chuang, K.-R.; Chen, S.-A. *Synth. Met.* **1996**, *82*, 159.
(24) Hagler, A. T. W.; Pakbaz, K.; Voss, F. K.; Heeger, A. J. *Phys. Rev. B* **1991**, *44*, 8652.
(25) Pichler, K.; Halliday, D. A.; Bradley, D. D.; Burn, P. L.; Friend, R. H.; Holmes, A. B. *J. Phys. Chem. Mater.* **1993**, *5*, 7155.
(26) Rothberg, L. J.; Yan, M.; Papadimitrakopoulos, F.; Galvin, M. E.; Kwock, E. W. *Synth. Met.* **1996**, *80*, 41.
(27) Munowitz, M. G.; Griffin, R. G.; Bodenhausen, G.; Huang, T. H. *J. Am. Chem. Soc.* **1981**, *103*, 2529.
(28) Lupton, J. M.; Samuel, I. D. W.; Monkman, A. P. *Synth. Met.* **1999**, *102*, 1079.
(29) Schaefer, J.; Stejskal, E. O.; Perchak, D.; Skolnick, J.; Yaris, R. *Macromolecules* **1985**, *18*, 368.
(30) Huster, D.; Xiao, L. S.; Hong, M. *Biochemistry* **2001**, *40*, 7662.
(31) Bonagamba, T. J.; Becker-Guedes, F.; DeAzevedo, E. R.; Schmidt-Rohr, K. *J. Polym. Sci., Part B: Polym. Phys.* **2001**, *39*, 2444.
(32) Becker-Guedes, F.; DeAzevedo, E. R.; Bonagamba, T. J.; Schmidt-Rohr, K. *Appl. Magn. Reson.*, in press.
(33) Talhavini, M.; Atvars, T. D. Z. *Quím. Nova* **1995**, *18*, 298.
(34) Liu, Y.; Liu, M. S.; Li, X.-C.; Jen, A. K.-Y. *Chem. Mater.* **1998**, *10*, 3301.
(35) Opella, S. J.; Frey, M. H. *J. Am. Chem. Soc.* **1979**, *101*, 5854.
(36) Vinogradov, E.; Madhu, P. K.; Vega, S. *Chem. Phys. Lett.* **1999**, *314*, 443.
(37) Bielecki, A.; Kolbert, A. C.; Levitt, M. H. *Chem. Phys. Lett.* **1989**, *155*, 341.
(38) Qing, Q. L.; Xuan, W.; Yong, F. *J. Appl. Phys.* **1992**, *72*, 4254.
(39) Chen, S.-H.; Su, A.-C.; Huang, Y.-F.; Su, C.-H.; Peng, G.-H.; Chen, S.-A. *Macromolecules* **2002**, *35*, 4229.
(40) Martins, T. D.; Yamaki, S. B.; Prado, E. A.; Atvars, T. D. Z. *J. Photochem. Photobiol. A: Chem.* **2003**, *153*, 91.
(41) Pierola, I. F.; Horta, A. *Rev. Iberamer. Polim.* **1992**, *1*, 49.

MA048340I